

## Research Article

# Locations of Satellite Galaxies in the Two-Degree Field Galaxy Redshift Survey

**Ingólfur Ágústsson and Tereasa G. Brainerd**

*Department of Astronomy, Boston University, 725 Commonwealth Avenue, Boston, MA, 02215, USA*

Correspondence should be addressed to Tereasa G. Brainerd, [brainerd@bu.edu](mailto:brainerd@bu.edu)

Received 24 June 2011; Accepted 8 August 2011

Academic Editors: J. A. L. Aguerri, E. Benitez, A. J. R. Sanderson, and W. W. Zeilinger

Copyright © 2011 I. Ágústsson and T. G. Brainerd. This is an open access article distributed under the Creative Commons Attribution License, which permits unrestricted use, distribution, and reproduction in any medium, provided the original work is properly cited.

We compute the locations of satellite galaxies in the Two-Degree Field Galaxy Redshift Survey using two sets of selection criteria and three sources of photometric data. Using the SuperCOSMOS  $r_F$  photometry, we find that the satellites are located preferentially near the major axes of their hosts, and the anisotropy is detected at a highly significant level (confidence levels of 99.6% to 99.9%). The locations of satellites that have high velocities relative to their hosts are statistically indistinguishable from the locations of satellites that have low velocities relative to their hosts. Additionally, satellites with passive star formation are distributed anisotropically about their hosts (99% confidence level), while the locations of star-forming satellites are consistent with an isotropic distribution. These two distributions are, however, statistically indistinguishable. Therefore it is not correct to interpret this as evidence that the locations of the star-forming satellites are intrinsically different from those of the passive satellites.

## 1. Introduction

The existence of massive halos of dark matter around large, bright galaxies is well accepted. However, at present there are relatively few direct observational constraints on the sizes and shapes of these dark matter halos. The most popular theory for structure formation in the universe, known as Cold Dark Matter (CDM), predicts that the dark matter halos extend to radii that are at least an order of magnitude greater than the radii of the visible galaxies (see, e.g., [1] and references therein). In addition, CDM predicts that the dark matter halos of galaxies are not spherical; instead they are triaxial in shape (e.g., [2–6]).

In principle, the locations of small, faint satellite galaxies, measured with respect to the major axes of the large, bright, “host” galaxies that they orbit, have the potential to provide strong constraints on the dark matter halos that surround the hosts, as well as on the relationships of the luminous hosts to their dark matter halos. Recent studies of satellite galaxies from modern redshift surveys have shown that, when their locations are averaged over the entire population, the satellites of relatively isolated host galaxies have a preference

for being located near the major axes of their hosts (e.g., [7–11]). The observed locations of the satellite galaxies in the Sloan Digital Sky Survey (SDSS; [12]) are also known to depend upon various physical properties of the hosts and satellites (e.g., [9, 11, 13]). The satellites of the SDSS host galaxies that have the reddest colors, highest stellar masses, and lowest specific star formation rates (SSFRs) show a pronounced tendency for being located near the major axes of their hosts. (Note: the SSFR has units of  $\text{yr}^{-1}$  and is defined to be the ratio of the star formation rate in the galaxy to its stellar mass; see [11].) On the other hand, the satellites of the SDSS host galaxies that have the bluest colors, lowest stellar masses, and highest SSFR are distributed isotropically around their hosts. The SDSS satellite galaxies that have the reddest colors, highest stellar masses, and lowest SSFR also show a strong preference for being located near the major axes of their hosts, while the SDSS satellite galaxies that have the bluest colors, lowest stellar masses, and highest SSFR show little to no anisotropy in their locations. The alignment of the satellites of relatively isolated SDSS host galaxies is also known to be similar to the alignment of satellites with the central galaxies of relatively isolated SDSS

galaxy groups, where the strongest alignment is found for red central galaxies and their red satellites, while no significant satellite alignment is detected for groups that have blue central galaxies (e.g., [14]).

From a theoretical standpoint, one would expect that if the dark matter halos of large, bright galaxies consist of CDM, then the locations of the satellite galaxies should reflect the deviations of the halo potentials from pure spherical symmetry. Simulations of structure formation in  $\Lambda$ CDM universes have shown that, in projection on the sky, the locations of the satellite galaxies trace the shapes of their hosts' dark matter halos rather well (e.g., [15]). However (and crucially), from an observational standpoint, the expected nonspherical distribution of satellite galaxies will only manifest in an observational data set if mass and light are reasonably well aligned within the hosts. In other words, the satellites should trace the dark mass associated with their hosts, but not necessarily the luminous mass associated with their hosts (i.e., since the dark mass exceeds the luminous mass by  $\sim 2$  orders of magnitude).

If the halos of the hosts are triaxial, and if one could simply use the symmetry axes of the hosts' dark matter halos (as projected on the sky) to define the geometry of the problem, one would naturally expect to observe an anisotropy in the locations of satellite galaxies such that the satellites are found preferentially close to the major axes of their hosts' dark matter halos. If there is a substantial misalignment between the projected major axes of the luminous host galaxies and their dark matter halos, however, one would expect to observe little to no anisotropy in the locations of the satellites. Using simple prescriptions for embedding luminous host galaxies within their dark matter halos [11] showed that the observed dependences of SDSS satellite locations on various host properties can be easily reproduced if mass and light are aligned in the elliptical hosts (i.e., luminous ellipticals are effectively miniature versions of their dark matter halos), while the disk hosts are instead oriented such that their angular momentum vectors are aligned with the net angular momentum vectors of their halos. The angular momentum alignment for the disk hosts and their halos introduces a significant misalignment of mass and light (e.g., [16]), resulting in the satellites of disk hosts being distributed much more isotropically than the satellites of elliptical hosts.

One of the difficulties with observational samples of host galaxies and their satellites is the presence of “interlopers” (i.e., “false” satellites) in the data. Since the distances to the galaxies are generally unknown, hosts and satellites are selected from redshift surveys via a set of redshift space proximity criteria. Typically, satellite galaxies must be located within a projected distance  $r_p \leq 500$  kpc of their host, and the line of sight velocity difference between a host and its satellite must be  $|\delta v| \leq 500$  km s<sup>-1</sup>. From simulations in which hosts and satellites were selected using criteria that are identical to the redshift space criteria used for observational data sets, it is known that the majority of objects that are selected as satellite galaxies are, in fact, located physically nearby a host galaxy. However, a substantial number of objects that are selected as satellites are located physically

far away from a host galaxy and are, therefore, interlopers (i.e., not genuine satellites; see [11]). When investigating the properties of the satellite population, the interlopers are a source of noise and ideally one would eliminate them from the sample if at all possible. This can be done in a simulation since the 3-dimensional locations of all of the objects are known, but it is not obvious how or if this can be accomplished in an observational data set.

So far, the only direct attempt to eliminate interlopers from an observational study of the locations of satellite galaxies is the work of [7]. In their study, [7] computed the locations of the satellites of relatively isolated host galaxies in the Two-Degree Field Galaxy Redshift Survey (2dFGRS; [17, 18]). In order to address the detrimental effects of interloper contamination, [7] argued that if they divided their host-satellite sample by relative line of sight velocity,  $|\delta v|$ , the set of host-satellite pairs that had the largest observed values of  $|\delta v|$  should suffer greater interloper contamination than the set of host-satellite pairs that had the smallest observed values of  $|\delta v|$ . That is, [7] anticipated that the peak of the observed relative velocity distribution,  $P(\delta v)$ , would be dominated by genuine satellites, while the tails of the distribution would be dominated by interlopers (for which the observed values of  $|\delta v|$  would be largely attributable to the Hubble flow). Therefore, [7] divided their sample of hosts and satellites into a “low relative velocity” sample ( $|\delta v| < 160$  km s<sup>-1</sup>) and a “high relative velocity” sample ( $|\delta v| > 160$  km s<sup>-1</sup>), expecting that the low relative velocity sample would suffer much less interloper contamination in comparison to the high relative velocity sample. Within both the full sample and the high relative velocity sample, [7] found no evidence for any anisotropy in the locations of the satellite galaxies. However, in the sample with  $|\delta v| < 160$  km s<sup>-1</sup>, [7] reported a preference for the satellites to be located near the major axes of their hosts (see [10], the erratum to [7]). Within this low relative velocity sample, [7] found that the ratio of “planar” ( $\phi < 30^\circ$ ) to “polar” ( $\phi > 60^\circ$ ) satellite locations was  $f = N_{<30}/N_{>60} = 1.25 \pm 0.06$  and that the distribution of satellite locations was fitted well by a double cosine function with amplitude  $A = 0.12 \pm 0.04$ .

In their analysis, the authors in [7] did not directly determine whether the results for the satellite locations in the low velocity sample were statistically distinct from the results for the satellite locations in the high velocity sample. That is, given the small number statistics with which the authors in [7] were working, it is entirely possible that the distribution of satellite locations in their high velocity sample was consistent with being drawn from the same parent population as the distribution of satellite locations in the low velocity sample. Therefore, it is not clear that their result should be interpreted as evidence that the satellites in the high velocity sample are distributed isotropically about their hosts, while the satellites in the low velocity sample are distributed anisotropically about their hosts. Rather, all that can be concluded about the high relative velocity sample in [7] is that the null hypothesis of a uniform distribution could not be ruled out. The fact that the null hypothesis could not be ruled out may be due to the locations of the satellites in the high velocity sample having an intrinsically

isotropic distribution. On the other hand, it could also be due to the size of the sample being too small to detect an intrinsic anisotropy in the presence of a significant amount of noise (i.e., this is a pair-counting problem that is dominated by  $\sqrt{N}$  statistics).

At the time the authors of [7] were doing their work, little was known about the distribution of the interlopers relative to the host galaxies and, for the most part, interlopers were simply assumed to be a population of objects that were selected at random (see, e.g., [19–21]). However, careful analysis of the interloper population from simulations has shown that the interlopers are far from being a random population. Instead, along the line of sight, most interlopers are located within a distance of  $\pm 2$  Mpc of a host (i.e., a distance far less than the  $\sim 7$  Mpc one would expect from the Hubble flow, given a maximum host-interloper velocity difference of  $|\delta v| = 500 \text{ km s}^{-1}$ ; see [22]). In addition, the probability distribution of relative velocities,  $P(\delta v)$ , for the hosts and interlopers reaches a maximum at  $\delta v = 0$  (e.g., [22, 23]). The distribution of relative velocities for host-interloper pairs is, in fact, quite similar to the distribution of relative velocities for pairs of hosts and their genuine satellites. Therefore, interlopers are almost as likely to have low velocities relative to the host galaxies as are the genuine satellites. In retrospect, then, it is not clear that the original velocity cut that [7] imposed in their analysis is well motivated, nor that there should be any significant difference in the locations of satellites with low velocities relative to their hosts and the locations of satellites with high velocities relative to their hosts.

Here we revisit the question of the locations of satellite galaxies in the 2dFGRS. We first adopt the selection criteria of [7] to obtain a host-satellite sample, and we compute the satellite locations using three different sets of photometry for the galaxies. We next adopt the selection criteria that we used in a previous study of the locations of satellite galaxies in the SDSS (e.g., [11]), and we focus our analysis on the hosts and satellites found using the SuperCOSMOS scans of the  $r_F$  plates. In all cases we determine whether the satellite locations in a low relative velocity sample of the data can be distinguished from the satellite locations in a high relative velocity sample. Finally, using the sample obtained with the SDSS selection criteria, we investigate the effect of star formation rate on the observed locations of the 2dFGRS satellites. Throughout we adopt cosmological parameters  $\Omega_{m0} = 0.25$ ,  $\Omega_{\Lambda 0} = 0.75$ , and  $H_0 = 73 \text{ km s}^{-1} \text{ Mpc}^{-1}$ .

## 2. Two-Degree Field Galaxy Redshift Survey

The Two-Degree Field Galaxy Redshift Survey (<http://msowwww.anu.edu.au/2dFGRS/>) is a publicly-available redshift survey that covers  $\sim 5\%$  of the sky. The target objects in the survey were selected in the  $b_J$  band from the Automated Plate Measuring (APM) galaxy survey and extensions to the survey (see [24, 25]). The photometry of the APM galaxy survey was based on scans of the UK Schmidt Telescope photographic survey plates obtained in blue ( $b_J$ ) and red ( $r_F$ ) spectral bands. Although the APM did not

complete the scans of the  $r_F$  plates, the SuperCOSMOS measuring machine was ultimately used to make independent scans of both the  $b_J$  and  $r_F$  plates (see [26, 27]); (<http://www-wfau.roe.ac.uk/sss/>). In addition to providing photometry in two spectral bands, [28] reports that the SuperCOSMOS scans yielded improved linearity and smaller random errors in comparison to the original APM scans. The final data release of the 2dFGRS contains 245 591 galaxies, of which 233 251 have good quality spectra ( $Q \geq 3$ ). Here we use the final 2dFGRS data release, and, specifically, we use the data for the best spectrum of each object (i.e., the ASCII catalog “*best.observations.idz*,” which contains the 2dFGRS spectral information, as well as the photometric information from the APM scans, for 231,178 sources with  $Q \geq 3$  and extinction-corrected magnitudes  $b_J \leq 19.45$ ). Additionally, we use the 2dFGRS database to retrieve the apparent magnitudes, the galaxy shape parameters (semimajor and semiminor axes), and the galaxy position angles for the SuperCOSMOS scans of the  $b_J$  and  $r_F$  plates.

Spectral types for the galaxies are quantified by the parameter  $\eta$ , which can be interpreted as an indicator of the amount of star formation in the galaxy (e.g., [29]). Rest-frame colors for the 2dFGRS galaxies can be obtained by using the relationship

$$(b_J - r_F)_0 = b_J - r_F - K(b_J) + K(r_F), \quad (1)$$

where  $K(b_J)$  and  $K(r_F)$  are color-dependent K-corrections from [30].

## 3. Locations of Satellites: Sample 1

We begin by obtaining hosts and satellites from the 2dFGRS using selection criteria that are identical to the criteria used by [7]. In selecting this host-satellite sample, we use the photometric parameters from the APM scans of the  $b_J$  plates, as did [7]. Here host galaxies must have redshifts  $z < 0.1$ , absolute magnitudes  $B_J < -18$ , and image ellipticities  $e = 1 - b/a \leq 0.1$ . In addition, host galaxies must be relatively isolated within their local regions of space. In order for a host to qualify as being relatively isolated, its  $B_J$  magnitude must be at least one magnitude brighter than any other galaxy that is found within a projected radius of  $r_p < 700 \text{ kpc}$  and line of sight velocity difference  $|\delta v| < 1000 \text{ km s}^{-1}$ . Satellites are galaxies that have absolute  $B_J$  magnitudes that are at least two magnitudes fainter than their host, are found within projected radii  $r_p < 500 \text{ kpc}$ , and have line of sight velocity differences  $|\delta v| < 500 \text{ km s}^{-1}$  relative to their hosts. In order to exclude host-satellite systems that are likely to be groups of galaxies, we reject all host-satellite systems that meet the above criteria, but which contain 5 or more satellites (see also [7]). After all of the above restrictions are imposed, our first sample consists of 1 725 hosts and 2 594 satellites. The size of our sample is slightly larger than that of [7] (which had 1 498 hosts), and the difference in sample size is likely attributable to small differences in the implementation of the selection criteria.

We define the location of a satellite,  $\phi$ , to be the angle between the major axis of its host galaxy and the direction

vector on the sky that connects the centroids of the host and satellite. Since we are only interested in determining whether the satellites are found preferentially close to either the major or minor axes of their hosts, we restrict  $\phi$  to the range  $0^\circ \leq \phi \leq 90^\circ$ . Therefore, “planar alignment” corresponds to a mean satellite location  $\langle \phi \rangle < 45^\circ$  and “polar alignment” corresponds to a mean satellite location  $\langle \phi \rangle > 45^\circ$ .

Shown in the top panels of Figure 1 are the differential and cumulative probability distributions for the satellite locations in our first sample ((a) and (b), resp.). Here the centroids of the hosts and satellites, as well as the position angles of the host galaxies, are taken from the APM scans of the  $b_J$  plates. Error bars for  $P(\phi)$  were computed using 1,000 bootstrap resamplings of the data. Also shown in the top panels of Figure 1 are the mean satellite location, the median satellite location, the confidence level at which the  $\chi^2$  test rejects a uniform distribution for  $P(\phi)$ , and the confidence level at which the Kolmogorov-Smirnov (KS) test rejects a uniform distribution for  $P(\phi \leq \phi_{\max})$ . From Figures 1(a) and 1(b), then, the satellite locations in our first sample are consistent with an isotropic distribution. Following [7] we also compute the planar-to-polar ratio,  $f = N_{<30}/N_{>60} = 1.08 \pm 0.05$ , which again is consistent with an isotropic distribution.

Next, and again following [7], we divide our first sample into a “low relative velocity” sample ( $|\delta v| < 160 \text{ km s}^{-1}$ ; 1,209 hosts and 1,514 satellites) and a “high relative velocity” sample ( $|\delta v| > 160 \text{ km s}^{-1}$ ; 855 hosts and 1,080 satellites), and we repeat the analysis above. Unlike [7], however, we find no statistically significant indication that the satellites in either velocity sample are distributed anisotropically around their hosts. Further, a two-sample KS test that compares  $P(\phi \leq \phi_{\max})$  for the low relative velocity sample to  $P(\phi \leq \phi_{\max})$  for the high relative velocity sample finds that the two distributions are statistically identical. That is, the two-sample KS test rejects the null hypothesis that the two distributions are drawn from the same parent distribution at a confidence level of 18%. We summarize our results in lines 1–3 of Table 1, where  $P_{\text{KS}}$  is the confidence level at which the KS test rejects a uniform distribution for the satellite locations,  $\langle \phi \rangle$  is the mean satellite location,  $\phi_{\text{med}}$  is the median satellite location, and  $f$  is the planar-to-polar ratio. The error bound on  $\langle \phi \rangle$  is the standard deviation in the mean, and the error bounds on  $\phi_{\text{med}}$  and  $f$  are 68% confidence bounds obtained from 2,000 bootstrap resamplings of the data.

Lastly, we repeat our analysis using the same hosts and satellites as above, but we now obtain the host galaxy position angles from the SuperCOSMOS scans of the  $b_J$  and  $r_F$  plates. Using the host position angles from the SuperCOSMOS scans has no effect on our conclusions above; in all cases the locations of the satellites are consistent with an isotropic distribution. We summarize our results for the locations of the satellites from the SuperCOSMOS scans in Table 1, lines 4–6 ( $b_J$ ) and lines 7–9 ( $r_F$ ). A two-sample KS test that compares  $P(\phi \leq \phi_{\max})$  for the low relative velocity sample to  $P(\phi \leq \phi_{\max})$  for the high relative velocity sample finds that, for the  $b_J$  SuperCOSMOS scans, the two distributions are statistically indistinguishable (KS rejection confidence

level of 63%). Similarly, a two-sample KS test that compares  $P(\phi \leq \phi_{\max})$  for the low relative velocity sample to  $P(\phi \leq \phi_{\max})$  for the high relative velocity sample finds that, for the  $r_F$  SuperCOSMOS scans, the two distributions are also statistically indistinguishable (KS rejection confidence level of 7%).

Therefore, at least in case of the selection criteria adopted by [7], our analysis finds that there is no statistically significant evidence that the 2dFGRS satellites are distributed anisotropically around their hosts. Further, we find that there is no statistically significant evidence that dividing the host-satellite sample by relative velocity (i.e., low versus high) results in different conclusions about the locations of the satellites.

#### 4. Locations of Satellites: Sample 2

In order to compare most directly with our previous work using SDSS galaxies, we next obtain a host-satellite sample from the 2dFGRS using the selection criteria from [11]. Since the SDSS results are based upon  $r$ -band imaging and also because the shapes of galaxies are generally smoother at longer wavelengths than they are at shorter wavelengths (i.e., the position angles of the host galaxies may be more accurate when measured at longer wavelengths), here we restrict our analysis to the SuperCOSMOS scans of the  $r_F$  plates. The selection criteria that we adopt are similar to the selection criteria that we used to obtain our first sample, but here they are somewhat more relaxed. Host galaxies must have  $r_F$  magnitudes that are at least one magnitude brighter than any other galaxy that is found within a projected radius  $r_p \leq 700 \text{ kpc}$  and a line of sight velocity difference  $|\delta v| \leq 1,000 \text{ km s}^{-1}$ . Satellite galaxies are objects that, relative to their hosts, are found within projected radii  $r_p \leq 500 \text{ kpc}$ , have line of sight velocity differences  $|\delta v| \leq 500 \text{ km s}^{-1}$ , and have  $r_F$  magnitudes that are at least two magnitudes fainter than their host. In addition, the luminosity of each host must exceed the sum total of the luminosities of its satellites, each host may have at most 9 satellites, and hosts are restricted to the redshift range  $0.01 \leq z \leq 0.15$ . We place no restrictions either on the ellipticities of the hosts’ images or on their absolute magnitudes. However, we do require that the hosts and satellites have good quality spectra ( $Q \geq 3$ ) and that the hosts have well-defined spectral parameters ( $\eta \neq -99.9$ ). The latter constraint helps to insure that the host galaxies have fairly regular shapes. This results in 2,947 host galaxies and 4,730 satellites in our second sample (i.e.,  $\sim 80\%$  larger than our first sample above).

We assign rest-frame colors to the 2dFGRS hosts and satellites using (1) above. Following [30] we define red galaxies to be those with rest-frame colors  $(b_J - r_F)_0 \geq 1.07$  and blue galaxies to be those with rest-frame colors  $(b_J - r_F)_0 < 1.07$ . Following [29] we use the value of  $\eta$  as a measure of the star formation rate within a galaxy, from which we define galaxies with  $\eta > -1.4$  to be “star-forming” and galaxies with  $\eta \leq -1.4$  to be “passive.” Although rest-frame color and star formation rate are strongly correlated (i.e., red galaxies tend to have low star formation rates, while blue galaxies tend to have high star formation rates) these

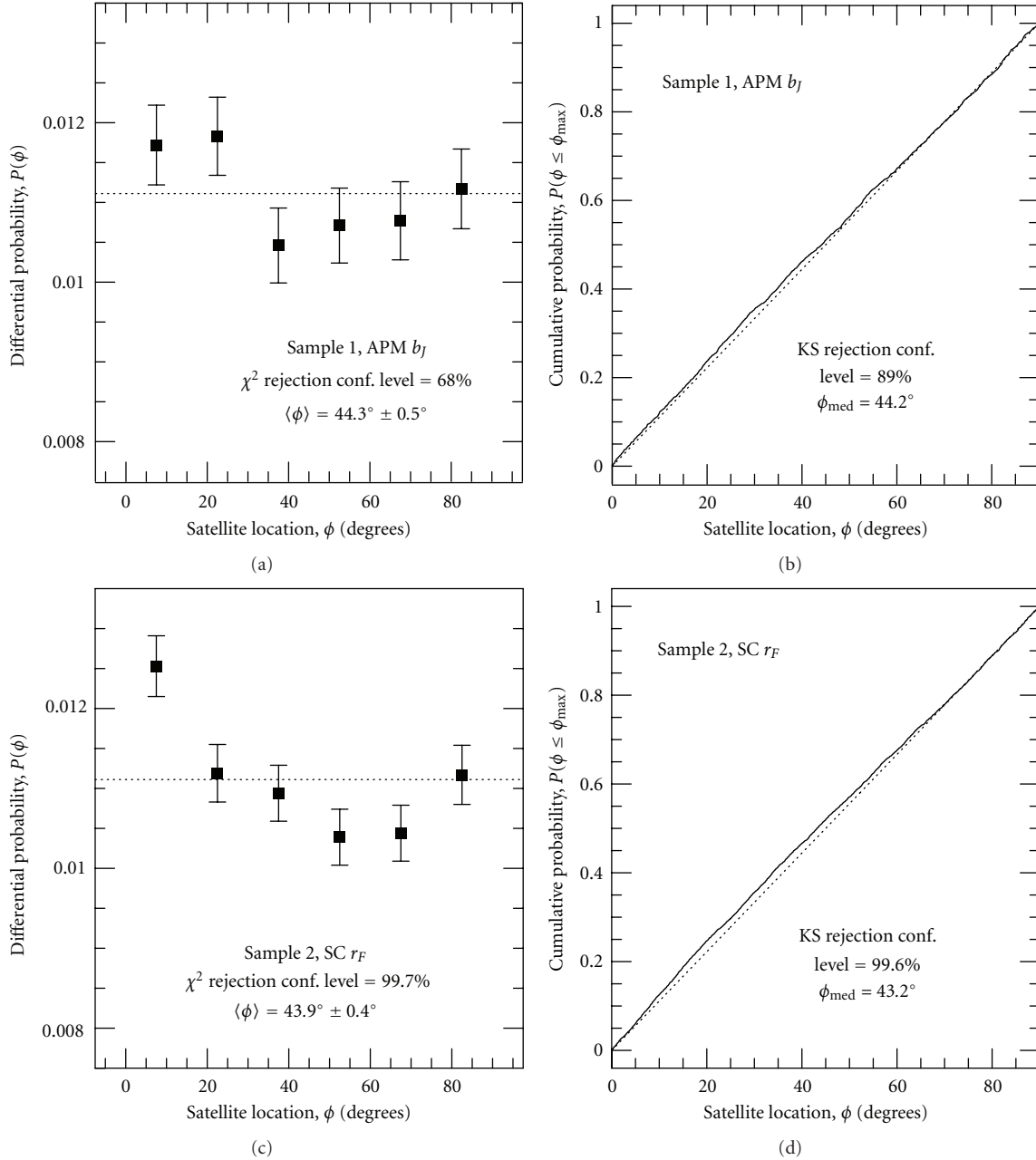


FIGURE 1: Probability distributions for the locations of satellite galaxies in the 2dFGRS. *Top.* Results for our first sample, where the APM scans of the  $b_j$  plates, the selection criteria from [7], and all host-satellite pairs are used in the calculations. *Bottom.* Results for our second sample, where the SuperCOSMOS scans of the  $r_F$  plates, the selection criteria from [11], and all host-satellite pairs are used in the calculations. *Left.* Observed differential probability distribution (data points with error bars). Dotted lines show the expectation for a uniform (i.e., isotropic) distribution. Also shown are the mean satellite location and the confidence level at which the  $\chi^2$  test rejects the uniform distribution. *Right.* Observed cumulative probability distribution (solid lines) and the expectation for a uniform distribution (dotted lines). Also shown are the median satellite location and the confidence level at which the KS test rejects the uniform distribution.

two parameters are not identical. Within our sample, 11% of the “passive” hosts have blue rest-frame colors and 28% of the “star-forming” hosts have red rest-frame colors. Of the 4,332 satellites that have well-defined spectral parameters, 13% of the “passive” satellites have blue rest-frame colors and 10% of the “star-forming” satellites have red rest-frame colors.

Figure 2 summarizes the basic statistical properties of the SuperCOSMOS  $r_F$  host-satellite sample obtained using the selection criteria of [11]. The different panels of Figure 2 show probability distributions for (a) the number of satellites per host, (b) the redshifts of the hosts, (c) the  $r_F$  apparent magnitudes of the hosts and satellites, (d) the  $r_F$  absolute magnitudes of the hosts and satellites, (e) the rest-frame

TABLE 1: Satellite locations in the 2dFGRS.

Sample	Scan	$ \delta v $	$P_{KS}$	$\langle \phi \rangle$ (degrees)	$\phi_{med}$ (degrees)	$f$
1	APM $b_J$	$< 500 \text{ km s}^{-1}$	89%	$44.3 \pm 0.5$	$44.2^{+0.7}_{-1.1}$	$1.08 \pm 0.05$
1	APM $b_J$	$< 160 \text{ km s}^{-1}$	91%	$44.0 \pm 0.7$	$43.9^{+0.9}_{-1.6}$	$1.11 \pm 0.07$
1	APM $b_J$	$> 160 \text{ km s}^{-1}$	9%	$44.7 \pm 0.8$	$44.7^{+1.2}_{-1.8}$	$1.04 \pm 0.08$
1	SC $b_J$	$< 500 \text{ km s}^{-1}$	86%	$44.3 \pm 0.5$	$44.0^{+1.0}_{-0.9}$	$1.08 \pm 0.05$
1	SC $b_J$	$< 160 \text{ km s}^{-1}$	90%	$43.8 \pm 0.7$	$43.3^{+0.9}_{-1.4}$	$1.13 \pm 0.07$
1	SC $b_J$	$> 160 \text{ km s}^{-1}$	6%	$44.9 \pm 0.8$	$45.3^{+2.0}_{-1.3}$	$1.00 \pm 0.08$
1	SC $r_F$	$< 500 \text{ km s}^{-1}$	90%	$44.4 \pm 0.5$	$44.1^{+0.9}_{-1.0}$	$1.10 \pm 0.05$
1	SC $r_F$	$< 160 \text{ km s}^{-1}$	83%	$44.4 \pm 0.7$	$43.8^{+1.3}_{-1.0}$	$1.10 \pm 0.07$
1	SC $r_F$	$> 160 \text{ km s}^{-1}$	31%	$44.5 \pm 0.8$	$44.3^{+1.6}_{-1.3}$	$1.08 \pm 0.08$
2	SC $r_F$	$< 500 \text{ km s}^{-1}$	99.6 %	$43.9 \pm 0.4$	$43.2^{+0.7}_{-0.5}$	$1.10 \pm 0.04$
2	SC $r_F$	$< 160 \text{ km s}^{-1}$	99.2%	$43.7 \pm 0.5$	$42.7^{+0.9}_{-1.0}$	$1.12 \pm 0.05$
2	SC $r_F$	$> 160 \text{ km s}^{-1}$	87%	$44.3 \pm 0.6$	$43.6^{+1.0}_{-0.7}$	$1.07 \pm 0.06$

colors of the hosts and satellites, and (f) the spectral types of the hosts and satellites. From Figure 2, then, our host sample is dominated by red, passive galaxies while our satellite sample is dominated by blue, star-forming galaxies. This is in good agreement with our previous results for the SDSS (e.g., [11]). For comparison, Figure 3 shows the basic statistical properties for the hosts and satellites of Sample 1 (see Section 3). Aside from differences that are due to different imposed cutoffs (i.e., maximum number of satellites and host galaxy redshift range), the statistical properties of the hosts and satellites are very similar for our two samples.

Probability distributions for the locations of all of the satellites in our second sample are shown in the bottom panels of Figure 1. The differential probability distribution,  $P(\phi)$ , is shown in Figure 1(c), along with the mean satellite location and the confidence level at which the  $\chi^2$  test rejects a uniform distribution for the satellites. The cumulative probability distribution,  $P(\phi \leq \phi_{max})$ , is shown in Figure 1(d), along with the median satellite location and the confidence level at which the KS test rejects a uniform distribution for the satellites. From Figures 1(c) and 1(d), then, the 2dFGRS satellites in our second sample are distributed anisotropically about their hosts, and the sense of the anisotropy is the same as the anisotropy of the SDSS satellites: when averaged over the entire sample, the satellites are located preferentially close to the major axes of their hosts. The significance of our detection of the anisotropy is, however, less for the locations of the 2dFGRS satellites ( $\chi^2$  and KS rejection confidence levels of 99.7% and 99.6%, resp.) than it was for the locations of the SDSS satellites in our previous study ( $\chi^2$  and KS rejection confidence levels  $> 99.99\%$ ; see [11]). This is likely due to a combination of effects. First, the host-satellite sample in [11] is  $\sim 50\%$  larger than the one we have used here (4,487 SDSS hosts and 7,399 SDSS satellites), which simply results in better statistics. Second, although the SDSS and 2dFGRS hosts have very similar redshift distributions, the images of the SDSS galaxies are somewhat better resolved than the images of the 2dFGRS galaxies (pixel size of 0.40 arcsec in the SDSS versus pixel size of 0.67 arcsec for the

SuperCOSMOS scans). This could lead to more accurate centroids for the SDSS galaxies, as well as more accurate position angles for the SDSS hosts. In addition, the rms velocity error in the 2dFGRS is  $\sim 85 \text{ km s}^{-1}$  (e.g., [17]), which is significantly greater than the  $\sim 30 \text{ km s}^{-1}$  rms velocity error in the SDSS (e.g., [31]). As a result, it would not be surprising if the 2dFGRS sample contains a larger fraction of interlopers than does the SDSS sample. The effect of interlopers is to reduce the observed anisotropy in the satellite locations (e.g., [11]). Hence, due to the smaller size of the 2dFGRS sample, the greater interloper contamination of the 2dFGRS sample, and the more accurate photometric parameters of the SDSS, we would naturally expect to find somewhat less anisotropy in the locations of the 2dFGRS satellites than in the locations of the SDSS satellites.

Next, using our second 2dFGRS host-satellite sample we again investigate whether dividing the sample into host-satellite pairs with low relative velocities ( $|\delta v| < 160 \text{ km s}^{-1}$ ; 1,988 hosts and 2,633 satellites) and high relative velocities ( $|\delta v| > 160 \text{ km s}^{-1}$ ; 1,512 hosts and 2,097 satellites) affects our ability to detect the anisotropy in the satellite locations. We summarize our results in Table 1, lines 10–12, from which it is clear that the anisotropy in the satellite locations is detected for the host-satellite pairs with low relative velocities (although, due to the smaller number of satellites, the significance is lower than it is for the full sample). In the case of the host-satellite pairs with high relative velocities, the satellite locations are consistent with an isotropic distribution (KS rejection confidence level of 87%). However, it is important to note that this alone does not constitute proof that the locations of the satellites in the high relative velocity sample are intrinsically different from the locations of the satellites in the low relative velocity sample (e.g., as might be expected if the high relative velocity sample contained a much larger fraction of interlopers than the low relative velocity sample).

In order to determine whether the satellite locations in the high relative velocity sample are truly different from those in the low relative velocity sample, we again compute

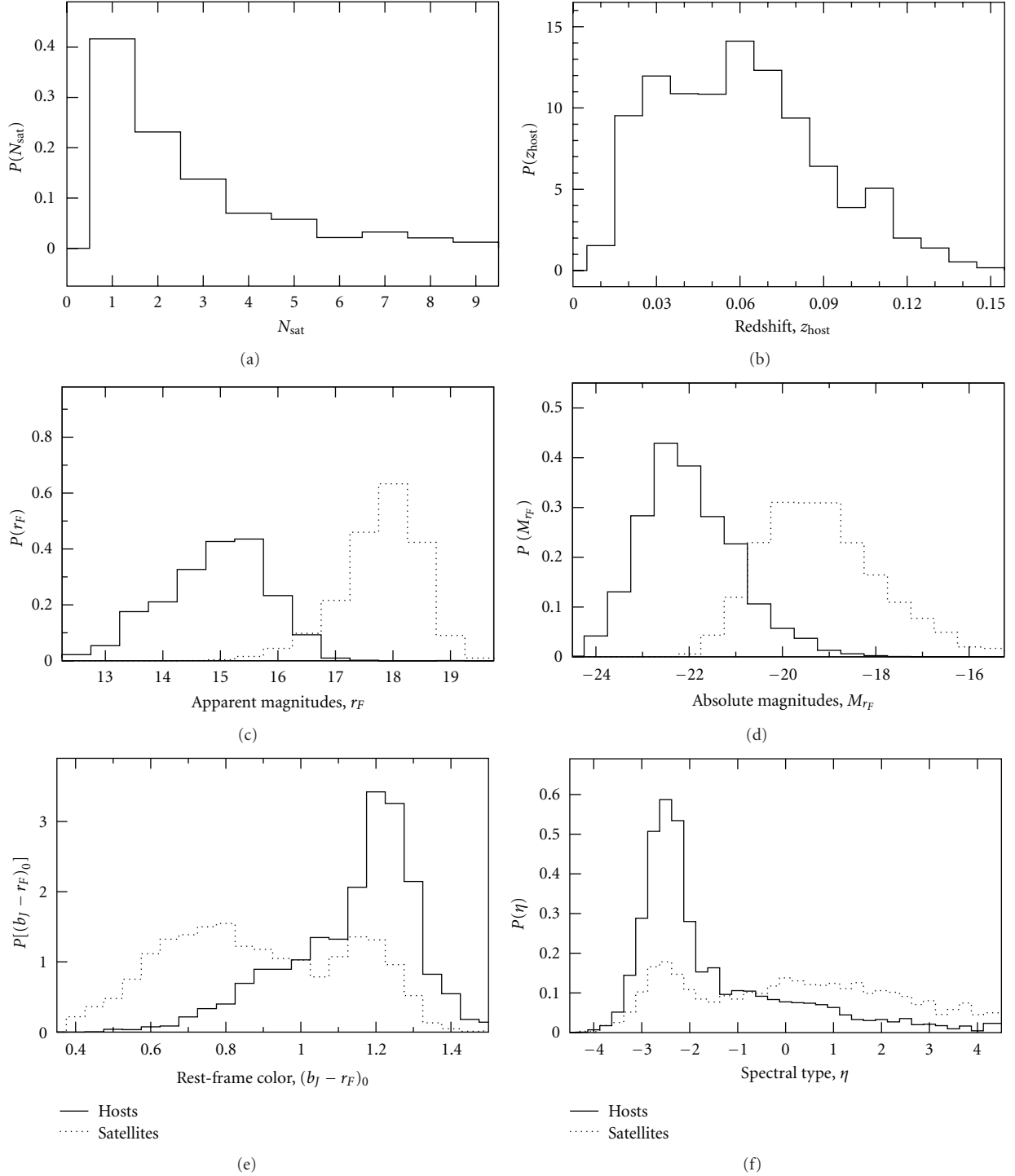


FIGURE 2: Statistical properties of Sample 2: (a) number of satellites per host, (b) host redshifts, (c)  $r_F$  apparent magnitudes of hosts (solid line) and satellites (dotted line), (d)  $r_F$  absolute magnitudes of hosts (solid line) and satellites (dotted line), (e) rest-frame colors of hosts (solid line) and satellites (dotted line), and (f) spectral types of hosts (solid line) and satellites (dotted line). Here the magnitudes have been obtained from the SuperCOSMOS scans.

a two-sample KS test. When we compare  $P(\phi \leq \phi_{\text{max}})$  for the high relative velocity sample to  $P(\phi \leq \phi_{\text{max}})$  for the low relative velocity sample, we find that the two distributions are statistically indistinguishable; the two-sample KS test rejects the null hypothesis that the two distributions are drawn

from the same distribution at a confidence level of 54%. Therefore, it is not correct to conclude that dividing our second sample by relative velocity yields one set of satellites that are distributed anisotropically about their hosts (i.e., the low relative velocity sample) and another set of satellites that

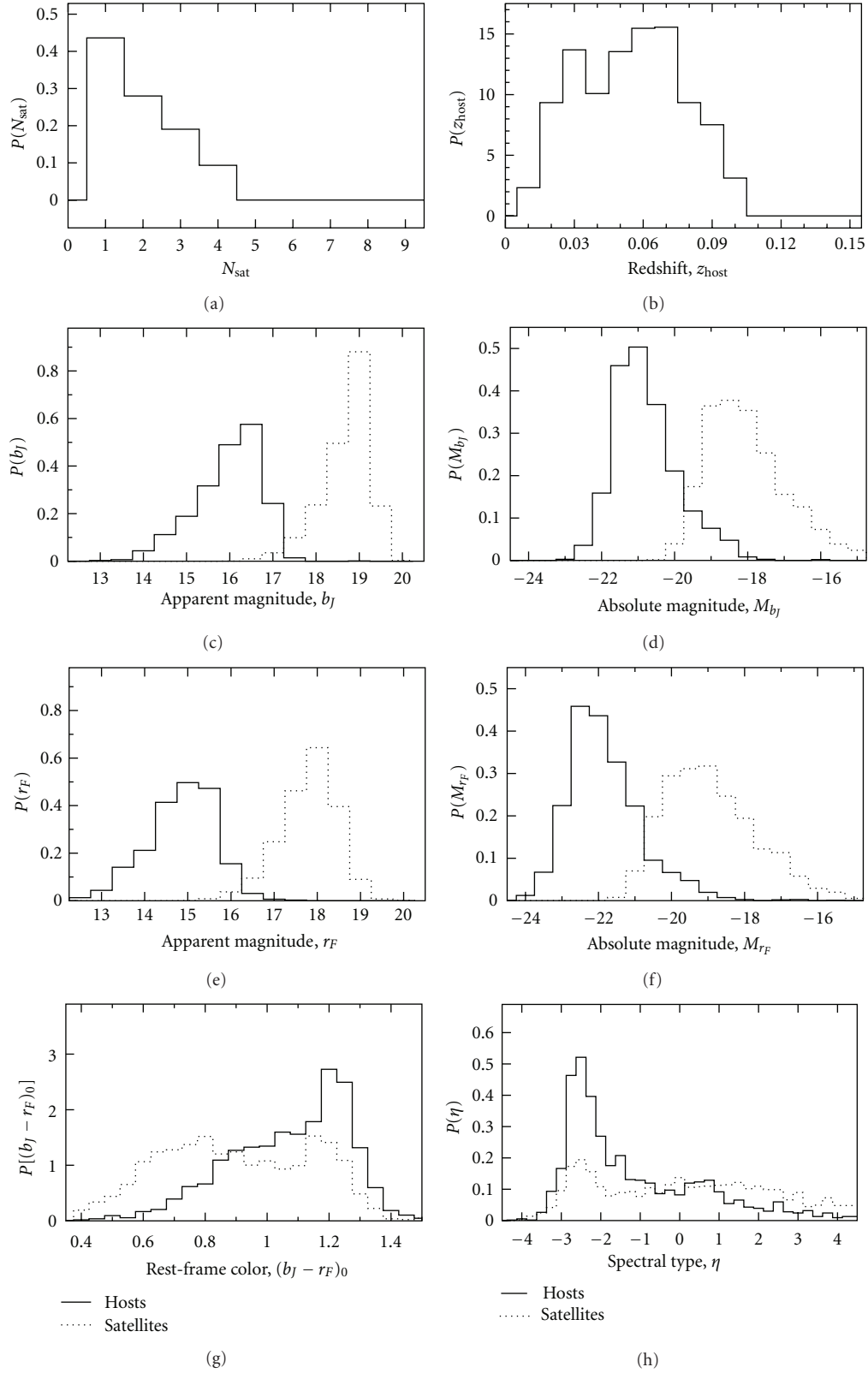


FIGURE 3: Statistical properties of Sample 1 for comparison to Sample 2: (a) number of satellites per host, (b) host redshifts, (c)  $b_J$  apparent magnitudes of hosts (solid line) and satellites (dotted line), (d)  $b_J$  absolute magnitudes of hosts (solid line) and satellites (dotted line), (e)  $r_F$  apparent magnitudes of hosts (solid line) and satellites (dotted line), (f)  $r_F$  absolute magnitudes of hosts (solid line) and satellites (dotted line), (g) rest-frame colors of hosts (solid line) and satellites (dotted line), and (h) spectral types of hosts (solid line) and satellites (dotted line). Here the magnitudes have been obtained from the SuperCOSMOS scans.

are distributed isotropically about their hosts (i.e., the high relative velocity sample).

At least for the rather small host-satellite sample that can be obtained from the 2dFGRS, it does not appear that dividing the sample by host-satellite relative velocity yields a substantial reduction in the effects of interloper contamination on the observed locations of the satellite galaxies. In other words, since  $P(\phi \leq \phi_{\max})$  for the high relative velocity sample is consistent with being drawn from the same distribution as  $P(\phi \leq \phi_{\max})$  for the low relative velocity sample, there is no statistically significant evidence that the satellites in the high relative velocity sample are distributed much more uniformly around their hosts than are the satellites in the low relative velocity sample. Both theoretically (e.g., [11, 22, 23]) and observationally, then, dividing the sample by host-satellite relative velocity does not obviously provide a significant reduction of the effects of interlopers on the observed locations of satellite galaxies.

If, however, we consider the star formation rates of the satellites, it could in principle be possible to identify a sample of satellites that contains both the smallest level of interloper contamination and the greatest degree of intrinsic anisotropy in the locations of the genuine satellites. From the theoretical work by [11], we know that the selection criteria that we have adopted here yield host galaxies that reside at the dynamical centers of large dark matter halos. The satellites are noncentral galaxies (i.e., “substructure”) that orbit within their hosts’ large dark matter halos. Prior to being accreted into the dark matter halo of its host galaxy, a satellite galaxy would have grown and evolved within its own dark matter halo. After accretion, the satellite would have ceased growing in mass and may have even lost mass (e.g., by tidal stripping when passing near the center of its hosts’ halo or by interactions with other subhalos). Star formation within the satellite would have been severely quenched after accretion by the host galaxy because the satellite loses most of its cold gas reservoir to the warmer, larger halo of its host. The higher the redshift at which a satellite was accreted, then, the lower should be its star formation rate at the present day, and the more likely its orbit will reflect the (nonspherical) gravitational potential of its host’s dark matter halo.

From [22], we know that by the present day (i.e.,  $z = 0$ ), only  $\sim 40\%$  of the genuine satellite galaxies in the Millennium Run Simulation (i.e., [1]) that have blue SDSS colors,  $(g - r)_0 < 0.7$ , have completed at least one orbit of their host galaxy. In contrast,  $\sim 86\%$  of the genuine satellite galaxies with red SDSS colors,  $(g - r)_0 \geq 0.7$ , have completed one or more orbits of their host galaxy by the present day. In addition, [11] found that when our selection criteria above were applied to the Millennium Run Simulation, only 42% of the objects with blue SDSS colors that were selected as satellites were, in fact, genuine satellites. However, [11] also found that 81% of the objects with red SDSS colors that were selected as satellites were actually genuine satellites. All in all, then, we would expect that an observational sample of satellite galaxies with low star formation rates and red SDSS colors should suffer the least amount of interloper contamination, while also exhibiting the greatest amount of intrinsic anisotropy in their locations relative to their hosts

(i.e., since they are relatively “old” satellites that have been within their hosts’ halos for a considerable length of time).

Due to the very small overlap of the 2dFGRS and the SDSS, SDSS colors are not available for more than a few objects in our sample. However, using the parameter  $\eta$  we can investigate the effects of star formation rate on the observed locations of the 2dFGRS satellites. If we classify the satellites with  $\eta > -1.4$  as “star forming” (3201 satellites) and  $\eta \leq -1.4$  as “passive” (1131 satellites), we then find that the cumulative probability distribution for the locations of the passive satellites is inconsistent with an isotropic distribution (KS rejection confidence level of 99%), while the cumulative probability distribution for the locations of the star-forming satellites is consistent with an isotropic distribution (KS rejection confidence level of 89.4%). In the case of the passive satellites,  $\langle \phi \rangle = 43.0^\circ \pm 0.8^\circ$  and  $\phi_{\text{med}} = 42.3_{-1.1}^{+1.2}$ , while for the star-forming satellites  $\langle \phi \rangle = 44.2^\circ \pm 0.5^\circ$  and  $\phi_{\text{med}} = 43.5^\circ \pm 0.7^\circ$ . As with the above results for the locations of satellites with high and low velocities relative to their hosts, however, this result should not be interpreted as evidence that the star-forming satellites are distributed isotropically about their hosts, while the passive satellites are distributed anisotropically about their hosts. Rather, a two-sample KS test finds that  $P(\phi \leq \phi_{\max})$  for the star-forming satellites is statistically indistinguishable from  $P(\phi \leq \phi_{\max})$  for the passive satellites (KS rejection confidence level 88.8%).

Finally, it is worth noting that, unlike our first sample, in our second sample we find a statistically significant detection of anisotropic satellite locations when we use the locations of all of the satellites in the analysis; that is, in our first sample, the satellite locations are consistent with an isotropic distribution. Given that our second sample is almost twice as large as our first sample, it is tempting to attribute the difference in the results from the two samples solely to improved statistics. However, the increase in the sample size does not appear to be the primary cause of the increased signal-to-noise. Instead, the selection of the hosts and satellites specifically using the SuperCOSMOS photometry seems to be the source of the improved signal-to-noise in our second sample.

If we simply restrict the analysis of our second sample to only those hosts that have  $z \leq 0.1$ , K-corrected SuperCOSMOS absolute magnitudes  $B_J < -18$ , ellipticities  $\epsilon > 0.1$  as measured from the  $r_F$  SuperCOSMOS photometry, and fewer than 5 satellites (i.e., to effectively match the selection criteria used to obtain our first sample), our second sample is substantially reduced in size: 2,089 hosts and 3,056 satellites. This restricted version of our second sample is only  $\sim 20\%$  larger than our first sample, which was selected using the APM scans of the  $b_J$  plates. This smaller, restricted  $r_F$  sample is substantially different from our  $b_J$  sample in Section 3 in that it includes only 1272 of the 1725 hosts in the  $b_J$  sample and only 1835 of the 2594 satellites in the  $b_J$  sample. Therefore,  $\sim 40\%$  of the hosts and satellites in the restricted  $r_F$  sample are not present in the  $b_J$ -selected sample from Section 3, and  $\sim 25\%$  of the hosts and satellites in the  $b_J$ -selected sample are not present in the restricted  $r_F$  sample.

When averaged over all satellites in the restricted version of our second sample, the locations of the satellites are

still inconsistent with an isotropic distribution (KS rejection confidence level of 99.9% and  $\chi^2$  rejection confidence level of 99.6%). Therefore, using the SuperCOSMOS scans of the  $r_F$  plates allows a detection of the anisotropic distribution of satellite galaxies that was not possible with the original APM scans of the  $b_J$  plates.

## 5. Summary

We have computed the locations of satellite galaxies in the 2dFGRS using two sets of selection criteria, and we have investigated whether dividing the sample by host-satellite relative velocity provides a significant reduction of the effects of interlopers on the observed locations of the satellites. When we adopt the selection criteria used by the authors of [7] in their study of the locations of 2dFGRS satellites, we find no statistically significant evidence that the satellites are distributed anisotropically about their hosts. This result is independent of the photometric catalogs that we use (APM scans of the  $b_J$  plates and SuperCOSMOS scans of the  $b_J$  and  $r_F$  plates), as well as the velocities of the satellites relative to their hosts. Our result is in contrast to the original study of [7], which found that the 2dFGRS satellites in the low relative velocity sample are distributed anisotropically around their hosts. The cause of this discrepancy is not clear, but it may lie in the fact that our samples are not truly identical or perhaps in differences in the way that the satellite locations were calculated in our independent analyzes.

We obtain a second host-satellite sample by applying a set of selection criteria that are based upon the criteria we used in a previous study of the locations of satellite galaxies in the SDSS. Further, our second sample is obtained using the  $r_F$  SuperCOSMOS photometry instead of the  $b_J$  APM photometry. Using our second sample, we find that the satellites are anisotropically distributed about their hosts at a statistically significant level (KS rejection confidence level of 99.6%). The sense of the anisotropy is in agreement with previous studies; when averaged over the entire population, the satellites have a preference to be found near the major axes of their host galaxies. When we divide our second sample into host-satellite pairs with low relative velocities ( $|\delta v| < 160 \text{ km s}^{-1}$ ) and host-satellite pairs with high relative velocities ( $|\delta v| > 160 \text{ km s}^{-1}$ ), we find that the satellites with low relative velocities are anisotropically distributed about their hosts at a statistically significant level, while an isotropic distribution cannot be ruled out for the locations of the satellites with high relative velocities. However, this result should not be interpreted as evidence that the distribution of the satellites in the low relative velocity sample is intrinsically different from that of the satellites in the high relative velocity sample. When we compare the distributions of the satellites in the low and high relative velocity samples, we find that they are statistically indistinguishable. As a result, it is not clear that dividing the sample by host-satellite relative velocity is a direct means of eliminating the effects of interlopers on the observed locations of satellite galaxies.

Although the selection criteria that we use to obtain our second sample result in a sample that is nearly twice as large as our first sample, the increase in the sample

size is not the primary reason that the anisotropy in the satellite locations can be detected in the second sample, but not the first. Instead, it is the improved photometry from the SuperCOSMOS scans of the  $r_F$  plates that leads to the increased signal-to-noise. If we restrict the analysis of our second sample to a set of host-satellite systems whose properties match those of our first sample, the second sample is only  $\sim 20\%$  larger than the first sample, yet the anisotropy of the satellite locations is detected at a highly significant level (KS rejection confidence level of 99.9%).

Finally, in an attempt to isolate a population of satellites that are likely to have the least interloper contamination, as well as the greatest degree of anisotropy in the locations of the genuine satellites, we investigated the effects of star formation rate on the locations of the 2dFGRS satellites. In our second sample, we find that passive satellites (which constitute only 26% of the satellites with well-defined spectral parameters) are distributed anisotropically around their hosts with high statistical significance (KS rejection confidence level of 99%). An isotropic distribution cannot be ruled out for the locations of the star-forming satellites. However, as with our result for dividing the sample by relative velocity, this should not be interpreted as evidence that the locations of the star-forming satellites around their hosts are intrinsically different from the locations of the passive satellites. Rather, we find that the two distributions of satellite locations are statistically indistinguishable in our 2dFGRS sample. Although the star formation rates are quantified differently in the SDSS than they are in the 2dFGRS (i.e., star formation is quantified by SSFR, not  $\eta$ , in the SDSS), this last result is in reasonable agreement with our previous results for satellite galaxies in the SDSS. That is, the SDSS satellites with the lowest SSFR show a pronounced tendency to be located near the major axes of their hosts, and the SDSS satellites with the highest SSFR show little anisotropy in their locations. However, the mean satellite locations,  $\langle \phi \rangle$ , for the SDSS satellites with the highest SSFR and the lowest SSFR agree with each other at the  $2\sigma$  level (see [11, Figure 1(c)]). Therefore, it is not clear that dividing the sample by the star formation rates of the satellites is sufficient to largely eliminate the effects of interlopers on the observed locations of satellite galaxies.

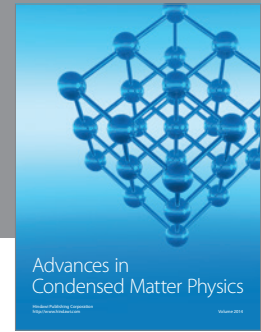
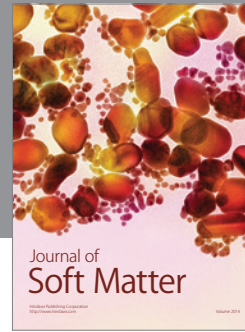
## Acknowledgments

The authors are pleased to thank all of those who were involved with the 2dFGRS. This work was supported by the National Science Foundation under NSF Contract AST-0708468.

## References

- [1] V. Springel, S. D. M. White, A. Jenkins et al., “Simulations of the formation, evolution and clustering of galaxies and quasars,” *Nature*, vol. 435, no. 7042, pp. 629–636, 2005.
- [2] M. S. Warren, P. J. Quinn, J. K. Salmon, and W. H. Zurek, “Dark halos formed via dissipationless collapse. I. Shapes and alignment of angular momentum,” *Astrophysical Journal*, vol. 399, no. 2, pp. 405–425, 1992.

- [3] Y. P. Jing and Y. Suto, "Triaxial modeling of halo density profiles with high-resolution N-body simulations," *Astrophysical Journal*, vol. 574, no. 2, pp. 538–553, 2002.
- [4] J. Bailin and M. Steinmetz, "Internal and external alignment of the shapes and angular momenta of  $\Lambda$ CDM halos," *Astrophysical Journal*, vol. 627, no. 2, pp. 647–665, 2005.
- [5] S. F. Kasun and A. E. Evrard, "Shapes and alignments of galaxy cluster halos," *Astrophysical Journal*, vol. 629, no. 2, pp. 781–790, 2005.
- [6] B. Allgood, R. A. Flores, J. R. Primack et al., "The shape of dark matter haloes: dependence on mass, redshift, radius and formation," *Monthly Notices of the Royal Astronomical Society*, vol. 367, no. 4, pp. 1781–1796, 2006.
- [7] L. Sales and D. G. Lambas, "Anisotropy in the distribution of satellites around primary galaxies in the 2dF Galaxy Redshift Survey: the Holmberg effect," *Monthly Notices of the Royal Astronomical Society*, vol. 348, no. 4, pp. 1236–1240, 2004.
- [8] T. G. Brainerd, "Anisotropic distribution of SDSS satellite galaxies: planar (not polar) alignment," *Astrophysical Journal*, vol. 628, no. 2, pp. L101–L104, 2005.
- [9] M. Azzaro, S. G. Patiri, F. Prada, and A. R. Zentner, "Angular distribution of satellite galaxies from the Sloan Digital Sky Survey Data Release 4," *Monthly Notices of the Royal Astronomical Society*, vol. 376, no. 1, pp. L43–L47, 2007.
- [10] L. Sales and D. G. Lambas, "Erratum: anisotropy in the distribution of satellites around primary galaxies in the 2dF Galaxy Redshift Survey: the Holmberg effect," *Monthly Notices of the Royal Astronomical Society*, vol. 395, no. 2, p. 1184, 2009.
- [11] I. Ágústsson and T. G. Brainerd, "Anisotropic locations of satellite galaxies: clues to the orientations of galaxies within their dark matter halos," *Astrophysical Journal*, vol. 709, no. 2, pp. 1321–1336, 2010.
- [12] K. N. Abazajian, J. K. Adelman-McCarthy, M. A. Agüeros et al., "The seventh data release of the Sloan Digital Sky Survey," *Astrophysical Journal, Supplement Series*, vol. 182, no. 2, pp. 543–558, 2009.
- [13] R. J. Siverd, B. S. Ryden, and B. S. Gaudi, "Galaxy orientation and alignment effects in the SDSS DR6," submitted to *The Astrophysical Journal*, <http://arxiv.org/abs/0903.2264>.
- [14] Y. Wang, X. Yang, H. J. Mo et al., "Probing the intrinsic shape and alignment of dark matter haloes using SDSS galaxy groups," *Monthly Notices of the Royal Astronomical Society*, vol. 385, no. 3, pp. 1511–1522, 2008.
- [15] I. Ágústsson and T. G. Brainerd, "The locations of satellite galaxies in a  $\Lambda$ CDM universe," *Astrophysical Journal*, vol. 650, no. 2, pp. 550–559, 2006.
- [16] P. Bett, V. Eke, C. S. Frenk, A. Jenkins, J. Helly, and J. Navarro, "The spin and shape of dark matter haloes in the Millennium simulation of a  $\Lambda$  cold dark matter universe," *Monthly Notices of the Royal Astronomical Society*, vol. 376, no. 1, pp. 215–232, 2007.
- [17] M. Colless, G. Dalton, S. Maddox et al., "The 2dF Galaxy Redshift Survey: spectra and redshifts," *Monthly Notices of the Royal Astronomical Society*, vol. 328, no. 4, pp. 1039–1063, 2001.
- [18] M. Colless, B. A. Peterson, C. Jackson et al., "The 2dF Galaxy Redshift Survey: final data release," preprint, <http://arxiv.org/abs/astro-ph/0306581>.
- [19] T. A. McKay, E. S. Sheldon, D. Johnston et al., "Dynamical confirmation of Sloan Digital Sky Survey weak-lensing scaling laws," *Astrophysical Journal*, vol. 571, no. 2, pp. L85–L88, 2002.
- [20] T. G. Brainerd and M. A. Specian, "Mass-to-light ratios of 2dF galaxies," *Astrophysical Journal*, vol. 593, no. 1, pp. L7–L10, 2003.
- [21] F. Prada, M. Vitvitska, A. Klypin et al., "Observing the dark matter density profile of isolated galaxies," *Astrophysical Journal*, vol. 598, no. 1, pp. 260–271, 2003.
- [22] I. Ágústsson, *Satellite galaxies as probes of dark matter halos*, Ph.D. thesis, Boston University, 2011.
- [23] F. C. van den Bosch, P. Norberg, H. J. Mo, and X. Yang, "Probing dark matter haloes with satellite kinematics," *Monthly Notices of the Royal Astronomical Society*, vol. 352, no. 4, pp. 1302–1314, 2004.
- [24] S. J. Maddox, G. Efstathiou, W. J. Sutherland, and J. Loveday, "The APM galaxy survey. I—APM measurements and star-galaxy separation," *Monthly Notices of the Royal Astronomical Society*, vol. 243, pp. 692–712, 1990.
- [25] S. J. Maddox, G. Efstathiou, and W. J. Sutherland, "The APM Galaxy Survey—part two—photometric corrections," *Monthly Notices of the Royal Astronomical Society*, vol. 246, no. 3, pp. 433–457, 1990.
- [26] N. C. Hambly, H. T. MacGillivray, M. A. Read et al., "The SuperCOSMOS Sky Survey—I. Introduction and description," *Monthly Notices of the Royal Astronomical Society*, vol. 326, no. 4, pp. 1279–1294, 2001.
- [27] N. C. Hambly, M. J. Irwin, and H. T. MacGillivray, "The SuperCOSMOS Sky Survey—II. Image detection, parametrization, classification and photometry," *Monthly Notices of the Royal Astronomical Society*, vol. 326, no. 4, pp. 1295–1314, 2001.
- [28] S. Cole, W. J. Percival, J. A. Peacock et al., "The 2dF Galaxy Redshift Survey: power-spectrum analysis of the final data set and cosmological implications," *Monthly Notices of the Royal Astronomical Society*, vol. 362, no. 2, pp. 505–534, 2005.
- [29] D. S. Madgwick, O. Lahav, I. K. Baldry et al., "The 2dF Galaxy Redshift Survey: galaxy luminosity functions per spectral type," *Monthly Notices of the Royal Astronomical Society*, vol. 333, no. 1, pp. 133–144, 2002.
- [30] V. Wild, J. A. Peacock, O. Lahav et al., "The 2dF Galaxy Redshift Survey: stochastic relative biasing between galaxy populations," *Monthly Notices of the Royal Astronomical Society*, vol. 356, no. 1, pp. 247–269, 2005.
- [31] M. A. Strauss, D. H. Weinberg, R. H. Lupton et al., "Spectroscopic target selection in the Sloan Digital Sky Survey: the main galaxy sample," *Astronomical Journal*, vol. 124, no. 3, pp. 1810–1824, 2002.



**Hindawi**

Submit your manuscripts at  
<http://www.hindawi.com>

